



Journal Name

ARTICLE

3D Hybrid perovskites solid solution: A facile approach for deposition of nanoparticles and thin films via B-site substitution

Muhammad Aamir,^a Rana Farhat Mehmood,^b Arshad Farooq Butt,^a Malik Dilshad Khan,^c Mohammad Azad Malik,^d Neerish Revaprasadu,^c Jean-Michel Nunzi,^e Muhammad Sher,^f and Javed Akhtar^{a*}

Received 00th January 20xx,
Accepted 00th January 20xx

DOI: 10.1039/x0xx00000x

www.rsc.org/

Mixed metal halide perovskite is gaining a paramount interest due to efficient band gap tunability and improved optical properties compared to their single metal halide perovskite. Compositional change in lead halide perovskite to explore the energy changes is thus valuable to try. Herein, we report the synthesis of a lead to lead free hybrid perovskite solid solution ($\text{CH}_3\text{NH}_3\text{Pb}_{1-x}\text{Cu}_x\text{Br}_3$) as nanoparticles and films. The increasing concentration of Cu^{2+} ions in the site of the Pb^{2+} ion in the perovskite shifted the diffraction peaks to a larger angle. Uniform spherically shaped nanoparticles were synthesized by a wet chemical method, the higher Cu^{2+} concentration leads to agglomeration, producing sheet like morphologies. However, the deposition of thin films of $\text{CH}_3\text{NH}_3\text{Pb}_{1-x}\text{Cu}_x\text{Br}_3$ perovskite solid solution shows that well defined morphologies begin to appear with increasing concentration of Cu^{2+} in the perovskite structure. The as-prepared bulk lead free $\text{CH}_3\text{NH}_3\text{CuBr}_3$ perovskite shows a band gap of 1.65 eV. A blue shift in photoluminescence (PL) was observed with copper enrich hybrid perovskites.

Introduction

The recent, robust development of perovskite materials has revolutionized the photovoltaics research field with the highest certified solar light conversion efficiency, reported to be over 20%.¹⁻⁴ Metal halide perovskites exhibit ideal properties for applications including photovoltaic,^{5, 6} sensing,⁷⁻⁹ photocatalysis,¹⁰ piezoelectric^{11, 12} and lasing¹³ due to a tunable band gap,^{14, 15} low exciton binding energy^{16, 17} and long carrier diffusion lengths^{18, 19} and broad band emission.^{20, 21} Despite the record efficiency, one major concern with this material is the toxicity of lead. Therefore, key challenge is to replace lead with less toxic metals, however, no compatible success has been reported so far.

Although, Pb has been replaced with its group members, Sn and Ge, but, the stability of the 2+ oxidation state decreases while moving up in the same group, which limits the use of these metals to synthesize stable metal halide perovskite. In

Particular, Sn has been widely studied as an alternative to Pb, but, it undergoes oxidation from Sn^{2+} to Sn^{4+} in which Sn^{4+} act as a p-type dopant by a self-doping process.²²⁻²⁴ The partial incorporation of Sn in the $\text{CH}_3\text{NH}_3\text{PbI}_3$ perovskite tune the optical properties.²³ Recently, Zhang *et al.*²⁵ have reported the gradual substitution of Sb^{3+} in the Pb^{2+} site of $\text{CH}_3\text{NH}_3\text{PbI}_3$ perovskite to tailor the optoelectronic property, and tuned the band gap from 1.55 eV to 2.06 eV. However, the complete interconversion of $\text{CH}_3\text{NH}_3\text{PbI}_3$ to the layered $\text{CH}_3\text{NH}_3\text{Sb}_{0.66}\text{I}_3$ perovskite leads to reduced photovoltaic efficiency. Only 1% Sb doping in $\text{CH}_3\text{NH}_3\text{PbI}_3$ was found to improve the Voc, FF and Isc of the solar cell.²⁵ These short comings drew the attention of the scientific community to explore other substitutes of Pb. Transition metals, where particularly attractive metals, such as, Fe^{2+} , Cu^{2+} etc. can be used to investigate potential alternatives to lead-based perovskites. Taking this into consideration there is an urge to develop an alternative transition metal based perovskite due to their chemical stability, reduced toxicity and abundance.

Herein, we have attempted for the first time, the synthesis, characterization and fabrication of nanoparticles and bulk perovskite solid solutions obtained by the incorporation of Cu^{2+} in the site of Pb^{2+} ions to produce the $\text{CH}_3\text{NH}_3\text{Pb}_{1-x}\text{Cu}_x\text{Br}_3$ series. The aim is to study the sequential effect on optical, morphological and structural properties which may provide a basis to optimize the conditions for photovoltaic applications of lead free $\text{CH}_3\text{NH}_3\text{CuBr}_3$.

Experimental

^a Materials laboratory, Department of Chemistry, Mirpur University of science & Technology (MUST), Mirpur-10250 (AJK), Pakistan. Email: javed.chem@must.edu.pk

^b Department of Chemistry, University of Education Lahore, Dera ghazi campus, Kangan Road, DG khan, Pakistan.

^c Department of Chemistry, University of Zululand, Private Bag X1001, Kwadlangezwa, 3886. South Africa.

^d School of Materials, The University of Manchester, Oxford Road, United Kingdom, M13 9PL. UK.

^e Department of chemistry, Queen's University, Kingston, ON K7L 3N6, Canada

^f Department of Chemistry, Allama Iqbal Open University, Islamabad, Pakistan

* Footnotes relating to the title and/or authors should appear here. Electronic Supplementary Information (ESI) available: [details of any supplementary information available should be included here]. See DOI: 10.1039/x0xx00000x

Materials

Lead bromide, copper bromide, methylamine, hydrogen bromide, diethyl ether, N, N dimethylformamide, acetone, octylamine and n-hexane were purchased from sigma Aldrich and used without further purification.

Characterizations

p-XRD measurements were performed using a Bruker aXS D8 advanced diffractometer with Cu-K α radiation ($\lambda = 1.5406 \text{ \AA}$) operated at 40 kV and 40 mA. Scanning electron microscopy (SEM) was carried out using a Philips XL30 FEG SEM. Energy-dispersive analysis of X-rays (EDAX) spectroscopy was performed using a DX4 detector. All samples were carbon coated using the Edwards coating system E306A prior to SEM analysis. A Perkin-Elmer Lambda 20 UV-vis spectrophotometer was used to carry out optical measurements in the 200-1100 nm wavelength range at room temperature. Samples were placed in quartz cuvettes (1 cm path length) and absorbance was recorded. Photoluminescence (PL) spectra were recorded on a Perkin-Elmer LS 55 luminescence spectrometer with xenon lamp over the range of 200-800 nm. The XPS spectra were measured on a Microlab 310-F spectrometer equipped with an XR-4 twin anode (Al/Mg). The manufacturer of this system is VG Scientific. The samples were mounted on a stub-type stainless steel holder using double-sided adhesive Cu tape and kept under high vacuum (10^{-8} mbar) overnight inside the preparation chamber before they were transferred into the analysis chamber (10^{-9} mbar) of the spectrometer. The XPS data were collected using MgK α radiation at 1253.6 eV (280 W, 14 kV) and a spherical sector analyzer (SSA) operating in CAE (constant analyzer energy) mode. Survey spectra were recorded from -5 to 1000 eV at a pass energy of 40 eV (number of scans: 5) using an energy step size of 2 eV. High resolution spectra were measured for C1s, N1s, Br3d, and Cu2p in the appropriate regions at a pass energy of 20 eV and an energy step size of 0.05 eV. The analyzed area on the specimens is about $5 \times 2 \text{ mm}^2$.

Synthesis of methylammonium bromide (CH₃NH₃Br)

The synthesis of methylammonium bromide was carried out by reacting 15.0 mL of methylamine (40% solution in water) and 20.0 mL of hydrogen bromide (48% solution in water) in a round bottom flask. The reaction was stirred for two hours in an ice bath. The solvent was evaporated using a rotary evaporator and recrystallized with ethanol. The obtained product was washed twice with diethyl ether and then dried at 60 °C for 24 hours.

Synthesis of CH₃NH₃Pb_{1-x}Cu_xBr₃ nanoparticles

The methylammonium lead bromide nanoparticles were synthesized by dissolving 0.0367 g (0.1mmol) of PbBr₂ and 0.0112 g (0.1mmol) of CH₃NH₃Br in 2.0 mL of octadecene with 1.0 mL of oleic acid and 0.0126g of octylammonium bromide at room temperature under stirring. The copper substitution was then performed by a successive increase of copper bromide by 20 %, while decreasing the amount of lead bromide by the same amount in the reaction mixture, keeping the CH₃NH₃Br/MBR₂ ratio constant at 1:1. After 2.0 minutes of reaction time, 10.0 mL of acetone was added in the reaction

mixture under stirring to obtain the precipitates. The obtained precipitates were then centrifuged at 10000 rpm for 10 minutes and then dispersed in hexane, followed by washing with acetone and centrifuged to get a colloidal suspension in toluene for further characterization.

Deposition of CH₃NH₃Pb_{1-x}Cu_xBr₃ thin films

To deposit perovskite bulk derivatives, the glass substrate was cleaned by sonicating for 15 minutes in a detergent, isopropanol and acetone, respectively. The 0.1 mM of perovskite was dissolved in 1.0 mL of DMF under stirring for 1 hour. The copper substitution in the CH₃NH₃PbBr₃ was carried out by adding a calculated amount of copper bromide by substituting the lead precursor in the reaction mixture. The as-prepared CH₃NH₃Pb_{1-x}Cu_xBr₃ perovskite derivatives were then spin coated at 3000 rpm for 30 second and then annealed at 100 °C for 10 minutes.

Results and discussion

The synthesis of nanoparticles and deposition of thin films of bulk CH₃NH₃Pb_{1-x}Cu_xBr₃ perovskites were carried out with an approach to develop lead free hybrid perovskite and to study their phase, shape and morphological effect. In the reactions to substitute copper in the lead based hybrid perovskite nanoparticles, copper bromide was added with lead bromide to control the concentration ratio of metal cations.

The CH₃NH₃PbBr₃ nanoparticles were yellow in color, but the Pb-site substitution with copper, the color of as-prepared nanoparticles started to change to green and then to violet on complete conversion to CH₃NH₃CuBr₃. In this study, the collection of CH₃NH₃CuBr₃ nanoparticles were unsuccessful. Repeated attempts to precipitate the nanoparticles by using different type of polar or non-polar solvents such as acetone, n-hexane, methanol, chloroform, cyclohexane and mixture of solvents, were unsuccessful.

Powder-XRD was performed to determine the effect of copper substitution on the crystalline structure of lead based hybrid perovskite. The as-prepared CH₃NH₃PbBr₃ nanoparticles showed diffraction peaks at $2\theta = 15.14^\circ$ (001), 21.39° (011), 30.35° (002), 34.01° (021), 37.35° (211), 43.31° (022), 46.08° (221) and 48.78° (031) representing the cubic phase of the perovskite structure as shown in Figure 1 (a). All observed peaks belong to the cubic phase of CH₃NH₃PbBr₃ with no extra phase and in agreement with the literature.^{14, 26} However, in the successive substitution of copper in the lead based perovskite, the diffraction peaks started shifting gradually from a lower angle to a higher angle. The concentrations of copper and the respective shift in the diffraction peaks is presented in Table 1. The shifting of the peaks is due to the smaller ionic size of the copper ion (ionic radii = 73 pm)²⁷ as compared to the lead (ionic radii 119 pm).²⁷ Figure 1 (b) shows the p-XRD spectra of nanoparticles with magnification of the peak centered near at $2\theta = 15^\circ$ and Figure 1 (c) shows the magnification of peak around $2\theta = 30^\circ$. These peaks belong to the (001) and (002) planes of the cubic CH₃NH₃PbBr₃ perovskite phase. The

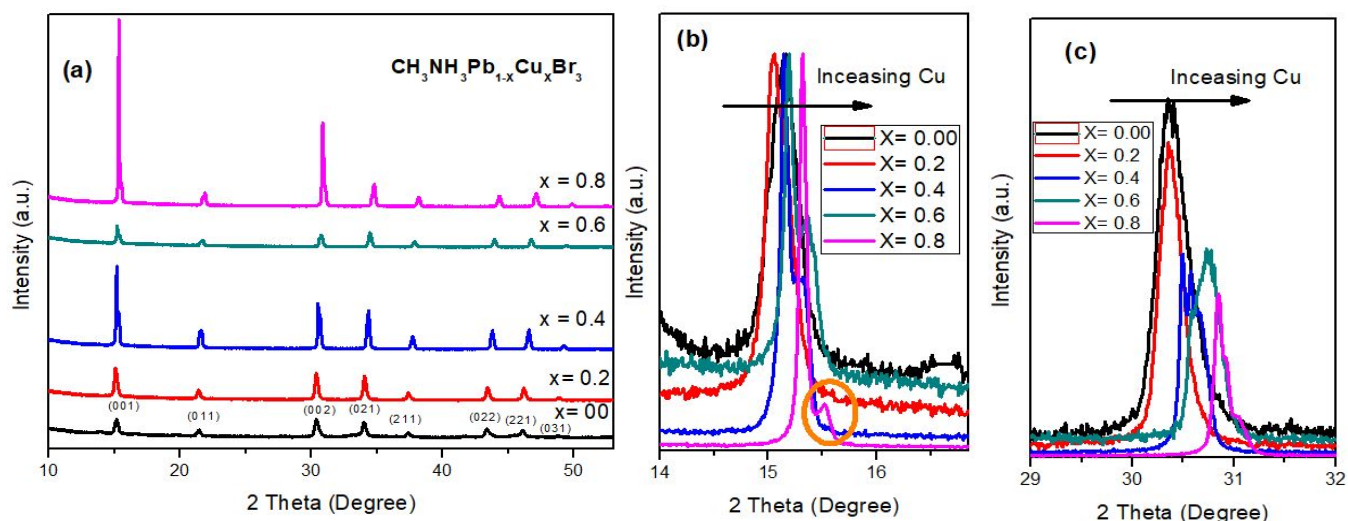


Figure 1. XRD spectra of the $\text{CH}_3\text{NH}_3\text{Pb}_{1-x}\text{Cu}_x\text{Br}_3$ nanoparticles by substituting Pb with Cu. (a) Complete spectra presenting the complete range of interest. (b, c) Magnifications of the peak centered at around 21.3° (b) and 30.3° (c).

prominent shifts in aforementioned diffraction peaks were observed, when Pb:Cu molar ratio was 0.6 : 0.4 ($\text{CH}_3\text{NH}_3\text{Pb}_{0.6}\text{Cu}_{0.4}\text{Br}_3$) as presented in Figure 1 (b-c). However, the shoulder peaks at $2\Theta = 15.31^\circ$ and 21.58° may be due to the phase segregation process.

Figure S1(a-f)(supporting information) shows the TEM images of the as-prepared nanoparticles of $\text{CH}_3\text{NH}_3\text{Pb}_{1-x}\text{Cu}_x\text{Br}_3$ hybrid perovskite derivatives. The nanoparticles synthesized at room temperature have uniform spherical morphology and are monodispersed with an average size of 12 ± 1 nm. The increase in molar ratio of Cu^{2+} and decrease in Pb^{2+} (Pb:Cu = 0.8:0.2, 0.6:0.4, 0.4:0.6, and 0.2:0.8) keeps the overall shape of particles as spherical (figure S1 a-e, supporting information). However, larger particles appeared due to the aggregation in $\text{CH}_3\text{NH}_3\text{Pb}_{0.6}\text{Cu}_{0.4}\text{Br}_3$, $\text{CH}_3\text{NH}_3\text{Pb}_{0.4}\text{Cu}_{0.6}\text{Br}_3$, and $\text{CH}_3\text{NH}_3\text{Pb}_{0.2}\text{Cu}_{0.8}\text{Br}_3$ (Figure S1 (c-e)). The copper addition may increase the rate of nucleation and enhance the growth of the nanoparticles, which results in larger particles. The complete conversion to $\text{CH}_3\text{NH}_3\text{CuBr}_3$ perovskite produced nanoparticles of more than 100 nm size with elongated shapes due to merging of smaller particles (Figure S1(f)). The inset in Figure S1 (f) shows that the $\text{CH}_3\text{NH}_3\text{CuBr}_3$ perovskite undergo anisotropic growth to form sheet like morphologies. These results suggest that the copper may facilitate faster nucleation and promotes large structure formation.

The optical properties of the as-synthesized nanoparticles of $\text{CH}_3\text{NH}_3\text{Pb}_{1-x}\text{Cu}_x\text{Br}_3$ perovskite derivatives were examined in detail with successive increase in copper concentration. During the conversion of $\text{CH}_3\text{NH}_3\text{PbBr}_3$ to lead free $\text{CH}_3\text{NH}_3\text{CuBr}_3$ perovskites, a slight change in absorption spectra was observed as shown in Figure S2 (a) (supporting information). Whereas, the main change was observed in photoluminescence (PL) as shown in Figure S2 (b) (supporting information). The $\text{CH}_3\text{NH}_3\text{PbBr}_3$ nanoparticles show a single emission peak at 508 nm. The emission intensity of this peak was decreased in $\text{CH}_3\text{NH}_3\text{Pb}_{0.8}\text{Cu}_{0.2}\text{Br}_3$ perovskite with the appearance of a new peak at 506 nm, which may be due to trap states generated by the copper ion. The gradual increase of copper ratio results in decrease of emission intensity peaked at 508 nm and slight blue shift in peak at 508 nm. In addition, a new peak at 392 nm was appeared for compound $\text{CH}_3\text{NH}_3\text{Pb}_{0.6}\text{Cu}_{0.4}\text{Br}_3$ along with blue shifted low intensity peak at 502 nm. In compound $\text{CH}_3\text{NH}_3\text{Pb}_{0.4}\text{Cu}_{0.6}\text{Br}_3$ three peaks were appeared, which were labelled at 492 nm, 444nm and 392 nm. These peaks were of low intensity suggesting that copper halide rich perovskite could be weak emitters. The PL emission spectra of $\text{CH}_3\text{NH}_3\text{Pb}_{0.2}\text{Cu}_{0.8}\text{Br}_3$ show multiple low intensity peaks located at 485 nm, 436 nm, 425 nm and 392 nm. However, in the $\text{CH}_3\text{NH}_3\text{CuBr}_3$ perovskite, the peaks at 485 nm disappeared with slight intense peaks at 425nm and 392 nm. The drop in PL intensity with increasing copper may be due to transformation

Table 1. p-XRD diffraction peaks of $\text{CH}_3\text{NH}_3\text{Pb}_{1-x}\text{Cu}_x\text{Br}_3$ perovskite derivatives.

Perovskite	Copper [x]	pXRD Diffraction peaks									
		(001)	----	(011)	----	(002)	(021)	(211)	(022)	(221)	(031)
$\text{CH}_3\text{NH}_3\text{PbBr}_3$	0	15.14°	----	21.39°	----	30.35°	34.01°	37.35°	43.31°	46.08°	48.78°
$\text{CH}_3\text{NH}_3\text{Pb}_{0.8}\text{Cu}_{0.2}\text{Br}_3$	0.2	15.05°	----	21.40°	----	30.35°	34.04°	37.40°	43.42°	46.18°	48.87°
$\text{CH}_3\text{NH}_3\text{Pb}_{0.6}\text{Cu}_{0.4}\text{Br}_3$	0.4	15.14°	15.31°	21.52°	21.58°	30.49°	34.35°	37.70°	43.77°	46.57°	49.26°
$\text{CH}_3\text{NH}_3\text{Pb}_{0.4}\text{Cu}_{0.6}\text{Br}_3$	0.6	15.19°	15.35°	21.54°	21.72°	30.72°	34.48°	37.83°	43.96°	46.77°	49.45°
$\text{CH}_3\text{NH}_3\text{Pb}_{0.2}\text{Cu}_{0.8}\text{Br}_3$	0.8	15.31°	15.51°	21.68°	21.89°	30.84°	34.77°	38.19°	44.31°	47.14°	49.86°

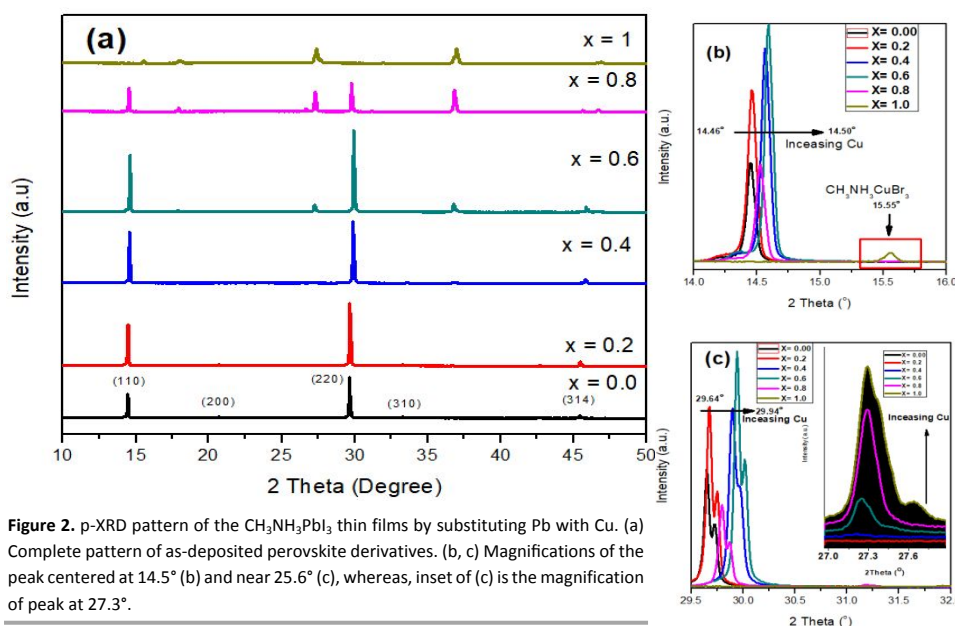


Figure 2. p-XRD pattern of the $\text{CH}_3\text{NH}_3\text{Pb}_{1-x}\text{Cu}_x\text{Br}_3$ thin films by substituting Pb with Cu. (a) Complete pattern of as-deposited perovskite derivatives. (b, c) Magnifications of the peak centered at 14.5° (b) and near 25.6° (c), whereas, inset of (c) is the magnification of peak at 27.3° .

of charge carries from lead based to copper based perovskite parts.

To further understand the structural and morphological evolution in B-site substituted hybrid perovskite using copper, we deposit the bulk $\text{CH}_3\text{NH}_3\text{Pb}_{1-x}\text{Cu}_x\text{Br}_3$ perovskite thin films using a single step spin coating method. The solution concentration was kept deliberately low, to understand the effect of copper substitution on the morphology and crystallization in as-prepared hybrid perovskite derivatives. Crystal structure analysis was performed by using p-XRD analysis as shown in Figure 2 (a). The diffraction peaks at $2\theta = 14.46^\circ, 20.70^\circ, 29.69^\circ, 33.36^\circ, 42.77^\circ$ and 45.49° were assigned to the (110), (200), (220), (310), (224) and (314) planes of the tetragonal perovskite phase of compound $\text{CH}_3\text{NH}_3\text{PbBr}_3$. The shifting of diffraction peaks to higher angles were observed with the increase of copper as shown in Figure 2b-c. Prominent changes in the diffraction peaks appears after Pb:Cu molar ratio of 0.6:0.4. Two new peaks appeared at $2\theta = 27.29^\circ$ and 36.85° in the diffraction patterns of $\text{CH}_3\text{NH}_3\text{Pb}_{0.6}\text{Cu}_{0.4}\text{Br}_3$, which were further intensified, as moving towards $\text{CH}_3\text{NH}_3\text{CuBr}_3$ end of the series. However, phase segregation was absent in bulk thin films.

The p-XRD pattern of $\text{CH}_3\text{NH}_3\text{CuBr}_3$ shows the complete absence of peaks at $2\theta = 29.69^\circ, 33.36^\circ, 42.77^\circ, 14.46^\circ$ and 20.70° which were observed in the lead based perovskite. Table 2 shows the change in diffraction peaks of $\text{CH}_3\text{NH}_3\text{Pb}_{1-x}\text{Cu}_x\text{Br}_3$ perovskite with the addition of copper ions.

Table 2. pXRD peak position in the bulk $\text{CH}_3\text{NH}_3\text{Pb}_{1-x}\text{Cu}_x\text{Br}_3$ perovskite derivatives thin films.

Perovskite	Copper [x]	pXRD Diffraction peaks								
		(110)	(200)	(220)	(310)	(224)	(314)	(224)	(314)	
$\text{CH}_3\text{NH}_3\text{PbBr}_3$	0	14.46°	20.70°	29.69°	33.36°	42.77°	45.49°
$\text{CH}_3\text{NH}_3\text{Pb}_{0.8}\text{Cu}_{0.2}\text{Br}_3$	0.2	14.48°	20.70°	29.72°	33.37°	45.54°
$\text{CH}_3\text{NH}_3\text{Pb}_{0.6}\text{Cu}_{0.4}\text{Br}_3$	0.4	14.49°	17.93°	27.29°	29.73°	33.41°	36.85°	45.55°
$\text{CH}_3\text{NH}_3\text{Pb}_{0.4}\text{Cu}_{0.6}\text{Br}_3$	0.6	14.50°	17.93°	27.29°	29.76°	36.85°	45.60°
$\text{CH}_3\text{NH}_3\text{Pb}_{0.2}\text{Cu}_{0.8}\text{Br}_3$	0.8	14.50°	17.93°	27.29°	29.76°	36.85°	34.77°
$\text{CH}_3\text{NH}_3\text{CuBr}_3$	0	17.93°	27.29°	36.85°

XPS measurements were recorded to determine the elemental composition and oxidation state of the Cu in $\text{CH}_3\text{NH}_3\text{CuBr}_3$ perovskite bulk films. The XPS spectrum for $\text{CH}_3\text{NH}_3\text{CuBr}_3$ shows peaks located at binding energies of 532 eV, 402 eV and 286 eV belonging to photoelectronic peaks of O1s, N1s and C1s respectively. Whereas, peaks around 930 eV and 69 eV corresponding to the Cu and Br, respectively. Figure 3 (a) shows the XPS spectra of C 1s binding energy for adventitious carbon (aliphatic).²⁸ After the linear background subtraction, the core level spectra were fitted using Gaussian line shapes. C 1s spectra of $\text{CH}_3\text{NH}_3\text{CuBr}_3$ demonstrate three peaks located at 284.93 eV, 285.78 eV and 286.64 eV. The peak at 284.93 eV is known as adventitious carbon or absorbed surface hydrocarbon from the atmosphere.²⁸ While, the peak at 285.78 eV belongs to the methyl carbons of $\text{CH}_3\text{NH}_3\text{CuBr}_3$ or possibly the methyl groups singly bonded to the hydroxyl group.²⁹ Another peak appeared at 286.64 eV corresponds to the carbon double bonded to oxygen, which also due to the surface contamination. Figure 3 (b) shows the XPS spectra of O 1s binding energy for $\text{CH}_3\text{NH}_3\text{CuBr}_3$ perovskite film. The O 1s have shown three peaks located at 531.08 eV, 532.04 eV, and 532.98 eV. Among these peaks, two peaks found at 531.08 eV and 532.98 eV corresponding to C=O, and O=C-O respectively.³⁰ These peaks typically appear in the air exposed samples and the carbons are known as adventitious carbons containing various hydrocarbon functionalities. The peak at 531.08 appeared mainly due to the weakly absorbed OH^- and O^{2-} ions, and can also be related to the Cu(II)-O/ Cu(OH)₂ like states.³¹ The formation of Cu(II)-O/ Cu(II)-OH like states indicate surface oxidation, where dissociated oxygen species or chemisorbed oxygen moieties can diffuse into the $\text{CH}_3\text{NH}_3\text{CuBr}_3$ structure that results in the distortion and degradation of the perovskite structure. Consequently, the decrease in the concentration of bromide ion at the surface of $\text{CH}_3\text{NH}_3\text{CuBr}_3$ film was observed. The atomic %

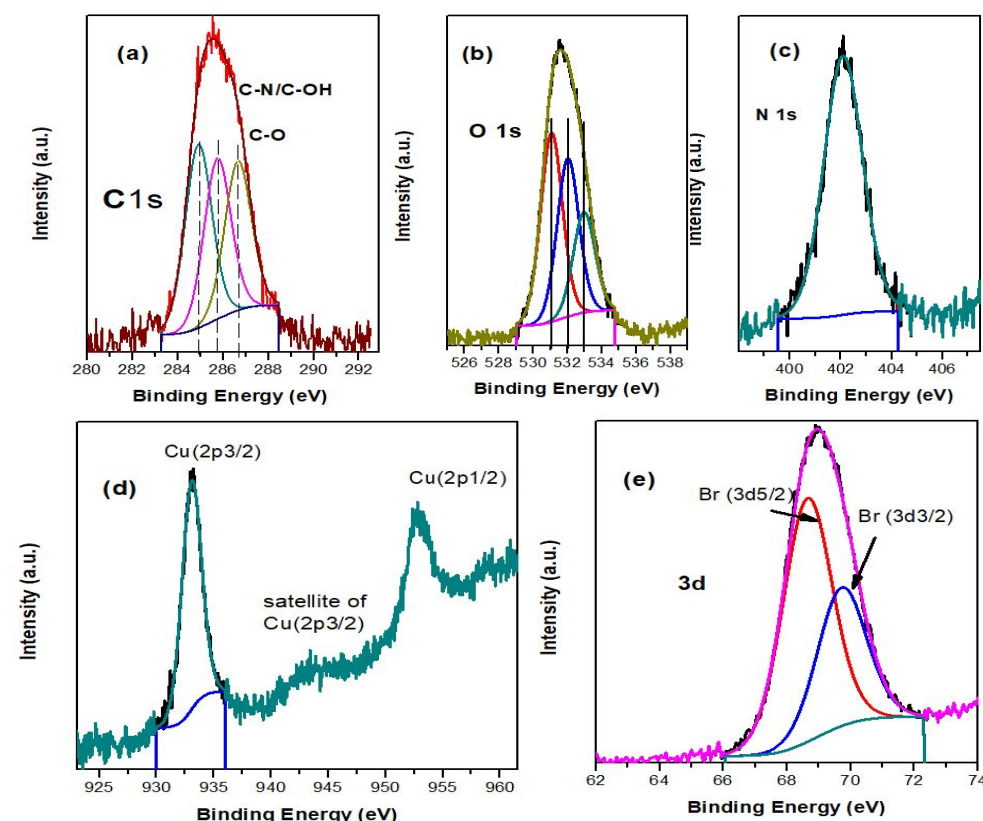


Figure 3. XPS analysis representing the electronic binding energies of (a) carbon, (b) oxygen, (c) nitrogen, (d) copper and (e) bromine in $\text{CH}_3\text{NH}_3\text{CuBr}_3$ perovskite.

of the $\text{CH}_3\text{NH}_3\text{CuBr}_3$ calculated by XPS shows around 25 % of oxygen moieties, which suggest that the as-deposited compound has easy diffusion of oxygen into the $\text{CH}_3\text{NH}_3\text{CuBr}_3$ thin film. The XPS spectra of N 1s show a characteristic peak located at binding energy of 402 eV (figure 3 (c)).

Figure 3 (d) shows the XPS spectra of Cu in $\text{CH}_3\text{NH}_3\text{CuBr}_3$ thin films. The Cu (2p_{3/2}) and Cu (2p_{1/2}) peaks positioned at 933.15eV and 952.73 eV respectively, which indicate the presence of Cu^{2+} . Furthermore, the satellite peak of Cu (2p_{3/2}) at 943.39 eV confirms the 2+ oxidation state of the copper.³¹ XPS spectra of core level Br 3d exhibits two peaks located at

68.68 eV and 69.77 eV corresponding to 3d_{5/2} and 3d_{3/2}, respectively (figure 3 (e)). The SEM images (Figure S3 (a-f) supporting information) of as-deposited thin films showed the significant change in morphology upon increase in copper in hybrid perovskite. The observation of flake-like grains of $\text{CH}_3\text{NH}_3\text{PbBr}_3$ crystallites shown in Figure S3 (a) and is well discussed in the literature.^{26, 32} The $\text{CH}_3\text{NH}_3\text{PbBr}_3$ perovskites flake-like grains can cover the surface of substrate to form uniform pinhole free thin films with a small modification in the deposition process. However, it was observed that more crystalline edges and crystal formation start to appear as Pb:Cu molar ratio was reached to 0.8:0.2 ($\text{CH}_3\text{NH}_3\text{Pb}_{0.8}\text{Cu}_{0.2}\text{Br}_3$ perovskite) as shown in Figure S3 (b) (supporting information). The increase in copper concentration produces cubic shaped morphologies (Figure S3 (b-d) (supporting information), however, when the molar ratio reaches to 0.4:0.6, some star shaped crystallites also appeared as shown in Figure S3 (d) (supporting information).

A flower-like growth of particles was observed in the thin film of $\text{CH}_3\text{NH}_3\text{Pb}_{0.2}\text{Cu}_{0.8}\text{Br}_3$ (Figure S3 (e) (supporting information)) with Pb:Cu molar ratio of 0.2:0.8, suggesting that the copper affects the morphology more effectively as compared to the lead ions. Finally, lead free $\text{CH}_3\text{NH}_3\text{CuBr}_3$ perovskite thin film shows small crystalline rice-like structures which were well dispersed on the glass substrate. The formation of these structures suggest that the copper based hybrid perovskite forms a crystal, which may lead to exposed surface of the glass

substrate and may result in thin films containing pinhole as shown in Figure S3 (f). This observation could provide a basis to optimize the deposition parameters to obtain the films with complete surface coverage during the fabrication of a $\text{CH}_3\text{NH}_3\text{CuBr}_3$ solar cell.

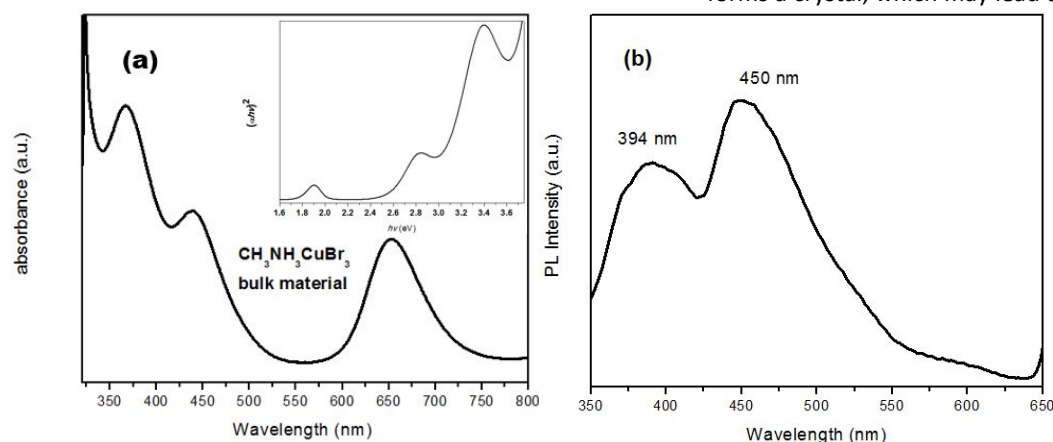


Figure 4. (a) UV-Vis absorption, inset is the Tauc plot and (b) PL spectra of bulk $\text{CH}_3\text{NH}_3\text{CuBr}_3$ perovskite.

UV-Vis absorption spectrum of the $\text{CH}_3\text{NH}_3\text{CuBr}_3$ perovskite is shown in Figure 4 (a). The

as-prepared compound $\text{CH}_3\text{NH}_3\text{CuBr}_3$ shows three distinct absorption peaks located at 653 nm, 438 nm and 367 nm. The appearance of three absorption peaks is probably due to the distortion of CuBr_6^- anion and the Jahn-Teller effect in this perovskite. In the inset of Figure 4 (a), the Tauc plot shows that the band gap of the as-synthesized $\text{CH}_3\text{NH}_3\text{CuBr}_3$ perovskite is about 1.65 eV, 2.53 eV and 2.93 eV. The 1.65 eV bandgap is close to the band gap of $\text{CH}_3\text{NH}_3\text{PbI}_3$ perovskite (1.55 eV).^{33, 34} Figure 4 (b) shows the PL emission spectrum of $\text{CH}_3\text{NH}_3\text{CuBr}_3$ perovskites excited at 330 nm, and two emission peaks located at 394 nm and 450 nm were observed. The appearance of two emission peaks may also arise due to the Jahn-Teller effect.

Conclusions

In summary, we have incorporated divalent Cu in the site of Pb in a hybrid perovskite to synthesize a solid solution of $\text{CH}_3\text{NH}_3\text{Pb}_{1-x}\text{Cu}_x\text{Br}_3$ in entire range, in the form of nanoparticles and thin films. It was observed that the gradual increasing of Cu^{2+} leads to a shift in the diffraction peaks to longer theta value, both in films and the nanoparticles. The uniform spherically shaped nanoparticles with sizes of 12 ± 1 nm were successfully synthesized using oleic acid as a capping agent. The increasing concentration of Cu^{2+} enlarges the size of the nanoparticles without effecting the shape. However, the films showed different morphologies with increasing Cu^{2+} concentration. The band gap of $\text{CH}_3\text{NH}_3\text{CuBr}_3$ perovskite was calculated to be 1.65 eV which found to be closer to $\text{CH}_3\text{NH}_3\text{PbI}_3$ perovskite (1.55 eV). In addition, the increasing Cu^{2+} amount also shifts the PL to shorter wavelength (blue shift). These results can provide a basis to establish lead free $\text{CH}_3\text{NH}_3\text{CuBr}_3$ perovskite as an alternative less toxic photovoltaic perovskite material.

Conflicts of interest

There are no conflicts to declare.

Acknowledgements

M. Aamir thanks higher education commission (HEC) of Pakistan for funding under start-up research grant program (SRGP) (Grant # 2262). JA acknowledges the funding from HEC, Pakistan under NRUP/R&D/2017-project #8227

References

1. A. Kojima, K. Teshima, Y. Shirai and T. Miyasaka, *J. Am. Chem. Soc.*, 2009, **131**, 6050-6051.
2. N. J. Jeon, J. H. Noh, W. S. Yang, Y. C. Kim, S. Ryu, J. Seo and S. I. Seok, *Nature*, 2015, **517**, 476-480.
3. M. Saliba, T. Matsui, J.-Y. Seo, K. Domanski, J.-P. Correa-Baena, M. K. Nazeeruddin, S. M. Zakeeruddin, W. Tress, A. Abate and A. Hagfeldt, *Energy Environ. Sci.*, 2016, **9**, 1989-1997.
4. M. Aamir, T. Adhikari, M. Sher, M. D. Khan, J. Akhtar and J. M. Nunzi, *Chem. Rec.*, 2018, **18**, 230-238.
5. M. Aamir, T. Adhikari, M. Sher, N. Revaprasadu, W. Khalid, J. Akhtar and J.-M. Nunzi, *New J. Chem.*, 2018, **42**, 14104-14110.
6. M. B. Johnston and L. M. Herz, *Acc. Chem. Res.*, 2015, **49**, 146-154.
7. M. Aamir, M. Sher, M. A. Malik, J. Akhtar and N. Revaprasadu, *New J. Chem.*, 2016, **40**, 9719-9724.
8. M. Aamir, M. Sher, M. A. Malik, N. Revaprasadu and J. Akhtar, *Mater. Lett.*, 2016, **183**, 135-138.
9. M. Aamir, M. D. Khan, M. Sher, S. V. Bhosale, M. A. Malik, J. Akhtar and N. Revaprasadu, *Eur. J. Inorg. Chem.*, 2017, **2017**, 3755-3760.
10. M. Aamir, Z. H. Shah, M. Sher, A. Iqbal, N. Revaprasadu, M. A. Malik and J. Akhtar, *Mater. Sci. Semicond. Process.*, 2017, **63**, 6-11.
11. Y.-M. You, W.-Q. Liao, D. Zhao, H.-Y. Ye, Y. Zhang, Q. Zhou, X. Niu, J. Wang, P.-F. Li and D.-W. Fu, *Science*, 2017, **357**, 306-309.
12. W.-Q. Liao, Y.-Y. Tang, P.-F. Li, Y.-M. You and R.-G. Xiong, *J. Am. Chem. Soc.*, 2017, **139**, 18071-18077.
13. S. Yakunin, L. Protesescu, F. Krieg, M. I. Bodnarchuk, G. Nedelcu, M. Humer, G. De Luca, M. Fiebig, W. Heiss and M. V. Kovalenko, *Nat. Commun.*, 2015, **6**.
14. T. Baikie, Y. Fang, J. M. Kadro, M. Schreyer, F. Wei, S. G. Mhaisalkar, M. Graetzel and T. J. White, *J. Mater. Chem. A*, 2013, **1**, 5628-5641.
15. G. E. Eperon, S. D. Stranks, C. Menelaou, M. B. Johnston, L. M. Herz and H. J. Snaith, *Energy Environ. Sci.*, 2014, **7**, 982-988.
16. C. S. Ponseca Jr, T. J. Savenije, M. Abdellah, K. Zheng, A. Yartsev, T. r. Pascher, T. Harlang, P. Chabera, T. Pullerits and A. Stepanov, *J. Am. Chem. Soc.*, 2014, **136**, 5189-5192.
17. A. Miyata, A. Mitioglu, P. Plochocka, O. Portugall, J. T.-W. Wang, S. D. Stranks, H. J. Snaith and R. J. Nicholas, *Nat. Phys.*, 2015, **11**, 582-587.
18. S. D. Stranks, G. E. Eperon, G. Grancini, C. Menelaou, M. J. Alcocer, T. Leijtens, L. M. Herz, A. Petrozza and H. J. Snaith, *Science*, 2013, **342**, 341-344.
19. G. Xing, N. Mathews, S. Sun, S. S. Lim, Y. M. Lam, M. Grätzel, S. Mhaisalkar and T. C. Sum, *Science*, 2013, **342**, 344-347.
20. M. Aamir, M. D. Khan, M. Sher, N. Revaprasadu, M. A. Malik and J. Akhtar, *New J. Chem.*, 2018, **42**, 17181-17184.
21. M. Aamir, M. D. Khan, M. Sher, M. A. Malik, J. Akhtar and N. Revaprasadu, *ChemistrySelect*, 2017, **2**, 5595-5599.
22. Q. Jiang, D. Rebollar, J. Gong, E. L. Piacentino, C. Zheng and T. Xu, *Angew. Chem.*, 2015, **127**, 7727-7730.
23. Y. Ogomi, A. Morita, S. Tsukamoto, T. Saitho, N. Fujikawa, Q. Shen, T. Toyoda, K. Yoshino, S. S. Pandey and T. Ma, *J. Phys. Chem. Lett.*, 2014, **5**, 1004-1011.
24. F. Hao, C. C. Stoumpos, D. H. Cao, R. P. Chang and M. G. Kanatzidis, *Nat. Photon.*, 2014, **8**, 489-494.
25. J. Zhang, M.-h. Shang, P. Wang, X. Huang, J. Xu, Z. Hu, Y. Zhu and L. Han, *ACS Energy Lett.*, 2016, **1**, 535-541.
26. R. Sheng, A. Ho-Baillie, S. Huang, S. Chen, X. Wen, X. Hao and M. A. Green, *J. Phys. Chem. C*, 2015, **119**, 3545-3549.
27. G. Kieslich, S. Sun and A. K. Cheetham, *Chem. Sci.*, 2015, **6**, 3430-3433.
28. A. L. Abdelhady, M. I. Saidaminov, B. Murali, V. Adinolfi, O.

Journal Name

ARTICLE

- 1
2
3 Voznyy, K. Katsiev, E. Alarousu, R. Comin, I. Dursun and L.
4 Sinatra, *J. Phys. Chem. Lett.*, 2016, **7**, 295-301.
5 29. S. Barman and M. Sadhukhan, *J. Mater. Chem.*, 2012, **22**,
6 21832-21837.
7 30. G. R. Kumar, A. D. Savariraj, S. Karthick, S. Selvam, B.
8 Balamuralitharan, H.-J. Kim, K. K. Viswanathan, M.
9 Vijaykumar and K. Prabakar, *Phys. Chem. Chem. Phys.*,
10 2016, **18**, 7284-7292.
11 31. I. L. Soroka, A. Shchukarev, M. Jonsson, N. V. Tarkina and
12 P. A. Korzhavyi, *Dalton Trans.*, 2013, **42**, 9585-9594.
13 32. G. E. Eperon, D. Bryant, J. Troughton, S. D. Stranks, M. B.
14 Johnston, T. Watson, D. A. Worsley and H. J. Snaith, *J. Phys.*
15 *Chem. Lett.*, 2014, **6**, 129-138.
16 33. M. A. Green, A. Ho-Baillie and H. J. Snaith, *Nat. Photon.*,
17 2014, **8**, 506-514.
18 34. T. C. Sum and N. Mathews, *Energy Environ. Sci.*, 2014, **7**,
19 2518-2534.
20
21
22
23
24
25
26
27
28
29
30
31
32
33
34
35
36
37
38
39
40
41
42
43
44
45
46
47
48
49
50
51
52
53
54
55
56
57
58
59
60

Supporting information

3D Hybrid perovskites solid solution: A facile approach for deposition of nanoparticles and thin films via B-site substitution

Muhammad Aamir, Rana Farhat Mehmood, Arshad Farooq Butt, Malik Dilshad Khan, Mohammad Azad Malik, Neerish Revaprasadu, Jean-Michel Nunzi, Muhammad Sher, and Javeed Akhtar *

Email: javeed.chem@must.edu.pk

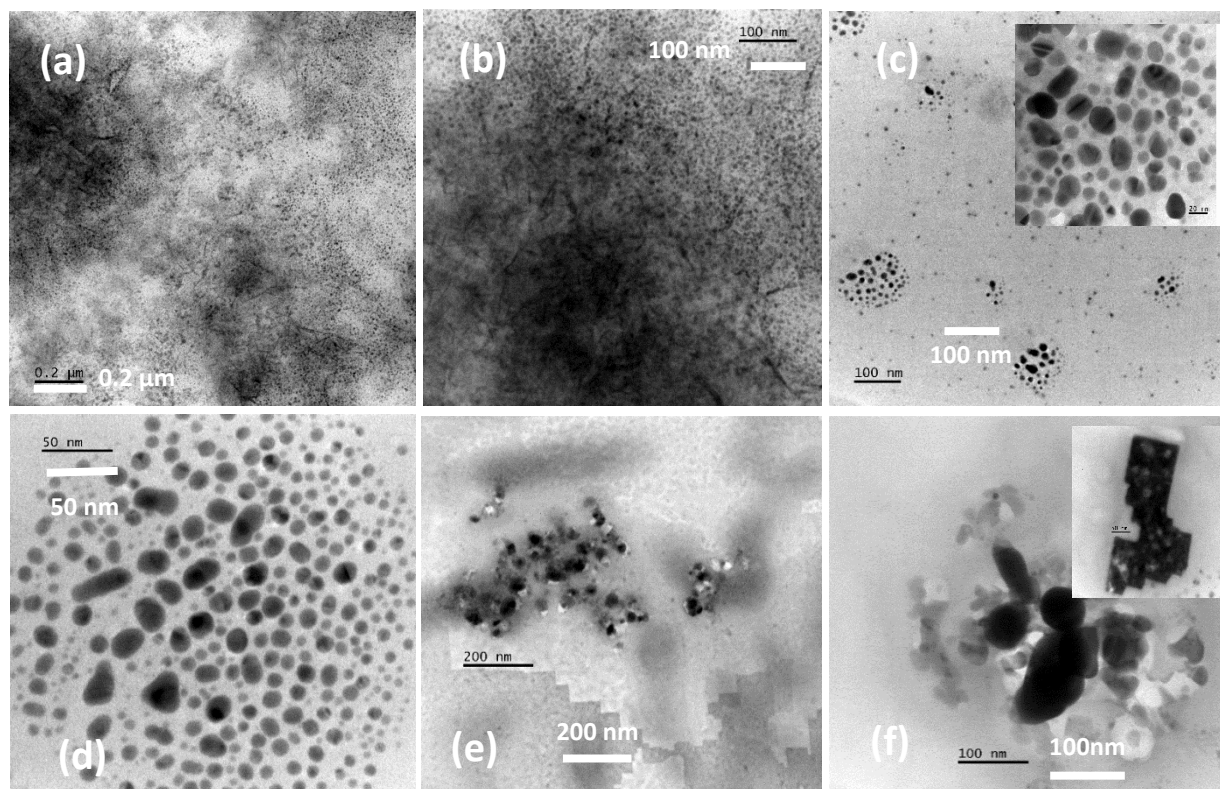


Figure S1. TEM images of as-prepared (a) CH₃NH₃PbBr₃, (b) CH₃NH₃Pb_{0.8}Cu_{0.2}Br₃, (c) CH₃NH₃Pb_{0.6}Cu_{0.4}Br₃, (d) CH₃NH₃Pb_{0.4}Cu_{0.6}Br₃, (e) CH₃NH₃Pb_{0.2}Cu_{0.8}Br₃ and (f) CH₃NH₃CuBr₃ perovskite nanoparticles at different magnifications

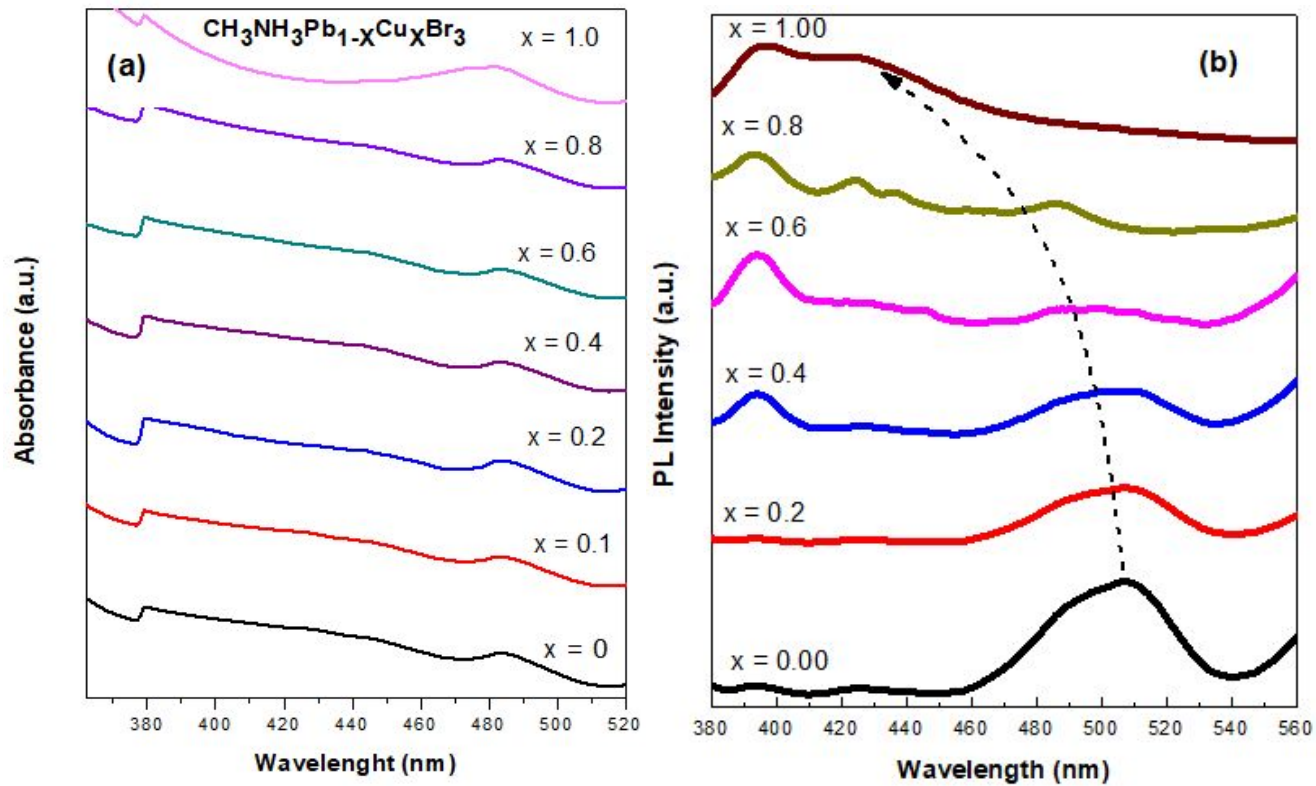


Figure S2. (a) UV-Vis spectra and (b) photoluminescence spectra of $\text{CH}_3\text{NH}_3\text{Pb}_{1-x}\text{Cu}_x\text{Br}_3$ perovskite nanoparticles.

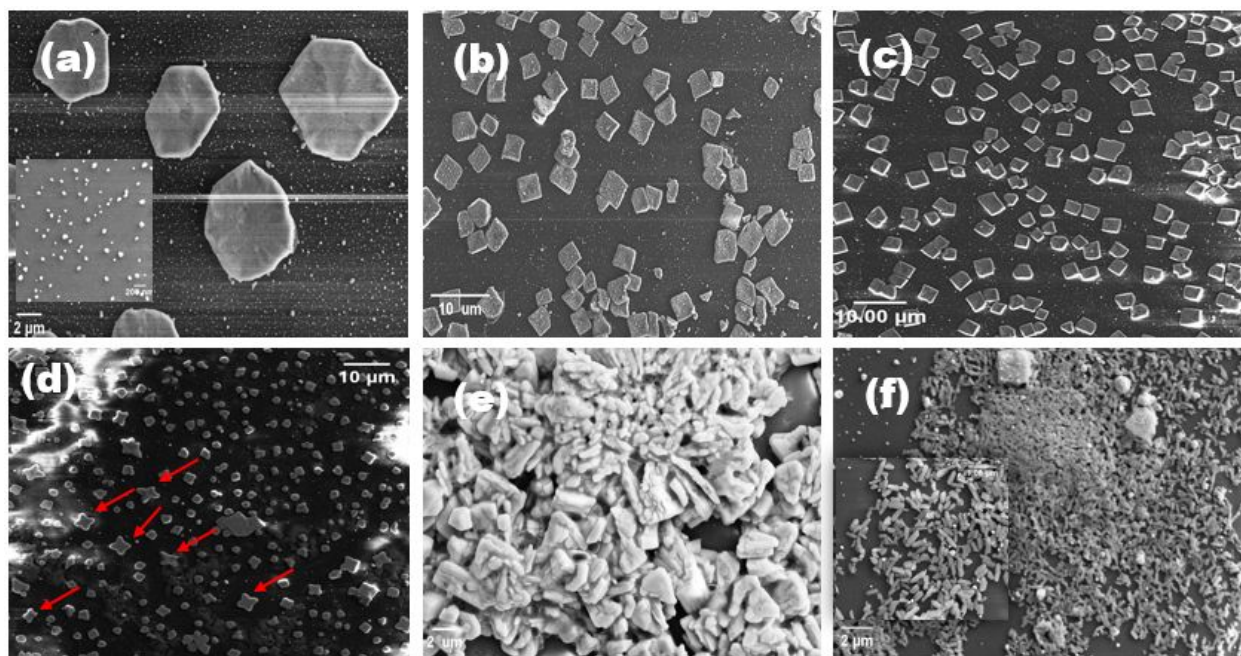


Figure S3. Field Emission Scanning Electron Microscopy images of as-synthesized (a) $\text{CH}_3\text{NH}_3\text{PbBr}_3$, (b) $\text{CH}_3\text{NH}_3\text{Pb}_{0.8}\text{Cu}_{0.2}\text{Br}_3$, (c) $\text{CH}_3\text{NH}_3\text{Pb}_{0.6}\text{Cu}_{0.4}\text{Br}_3$, (d) $\text{CH}_3\text{NH}_3\text{Pb}_{0.4}\text{Cu}_{0.6}\text{Br}_3$, (e) $\text{CH}_3\text{NH}_3\text{Pb}_{0.2}\text{Cu}_{0.8}\text{Br}_3$, and (f) $\text{CH}_3\text{NH}_3\text{CuBr}_3$ at different magnifications.